

Static light scattering properties of a ZnO nanosphere aqueous suspension at visible and near-infrared wavelengths

Haopeng Wu (武浩鹏)^{1,2}, Jiulin Shi (史久林)^{1,2,*}, Feng Yan (严峰)^{1,2},
Junjie Yang (杨俊杰)^{1,2}, Yubao Zhang (张余宝)^{1,2}, and Xingdao He (何兴道)^{1,2,**}

¹Jiangxi Engineering Laboratory for Optoelectronics Testing Technology, Nanchang Hangkong University, Nanchang 330063, China

²National Engineering Laboratory for Nondestructive testing and Optoelectric Sensing Technology and Application, Nanchang Hangkong University, Nanchang 330063, China

*Corresponding author: hyq1304@126.com; **corresponding author: xingdaohe@126.com

Received September 6, 2016; accepted November 11, 2016; posted online December 21, 2016

The scattering properties of ZnO nanospheres with four different particle diameters of 10, 50, 100, and 200 nm suspended in water are investigated theoretically and experimentally in the spectral range of the entire visible range and part of the near-infrared region. The scattering properties of ZnO nanospheres suspended in water are described by employing three main parameters: the angular distribution of the scattering intensity I , the scattering extinction coefficient α_{scat} , and the scattering cross section σ_{scat} . The results indicate that (i) at a certain wavelength, the angular distribution of the scattering intensity appears as an obviously forward-propagating feature, and the forward-scattering intensity is dominant gradually when the particle diameter increases from 10 to 200 nm, and (ii) the scattering extinction coefficient and cross section can be determined by using the measured transmittance changes of a pure water sample and a given ZnO sample; they all are shown to be dependent on the particle size and incident wavelength. The experimental results of four different scattering samples agree well with the theoretical predictions within the given wavelength range.

OCIS codes: 290.5850, 290.5820, 290.5825.

doi: 10.3788/COL201715.012901.

Light scattering has been a topic of widespread attention in the fields of fundamental research and practical applications. Generally, the scattering of light may occur when an incident light beam encounters an obstacle or any kind of fluctuations of spatial or temporal properties of a given medium. It is generally known that light scattering has been categorized usually as one of the following three types in terms of the incident light wavelength and the particle size of scattering medium: Rayleigh, Mie, and Tyndall scatterings^[1-3].

Scientists have long been intrigued with the discussion of some observable scattering phenomena from various particles, such as rainbows, the blue sky, and the orange sunset. Some advanced theories and efficient computational methods have been developed for explaining these and related phenomena over the years^[4-8]. Furthermore, the interests and objectives behind these developments have varied during the last decade, and new driving forces have emerged due to the advent of some new materials. For example, the increasing attention on the “nanoworld” has boosted the interest in the unique realm of nanoparticles and has afforded a new opportunity for researching the scattering properties of nanoparticle systems^[9-11]. Nowadays, much interest is focused on nanoparticle systems and the interaction effect between a scattering particle and its surrounding medium^[12-18]. Typically, light scattering is measured usually from a system of nanoparticles suspended in liquids, most often aqueous. The size,

structure, shape, composition, and average refractive index of the particles are often readily determined by analyzing the scattering data collected. For a further understanding of the behaviors presented by various types of nanoparticles, it is helpful to study marine optics, space optics, and biomedical optics^[19-21].

In this work, we present the scattering behaviors of ZnO nanospheres of different sizes ranging from 10 to 200 nm suspended in water theoretically and experimentally. ZnO nanospheres dispersed in water were chosen for the investigation in this work because they exhibit high stability, and patent thermodynamic, electromagnetic, electrodynamic, and optical properties, as well as being easy to prepare^[22,23]. The results of the theoretical simulations and experimental measurements of the extinction and scattering cross sections for ZnO nanospheres dispersed in water are conducive to studying low-threshold stimulated emission, random laser emission, and so on^[24,25]. In addition, it may be helpful to study the refractive index change behavior of nanoparticles suspended in a liquid medium. All these features make the investigation of the scattering behaviors of ZnO nanospheres very interesting.

The samples for this scattering experiment were ZnO nanospheres (Beijing DK nano technology Co.LTD) dispersed in water. Shown in Figs. 1(a) and 1(b) are the transmission electron microscope (TEM) image of the ZnO nanospheres and the transmission and absorption spectra of the ZnO nanosphere samples with different

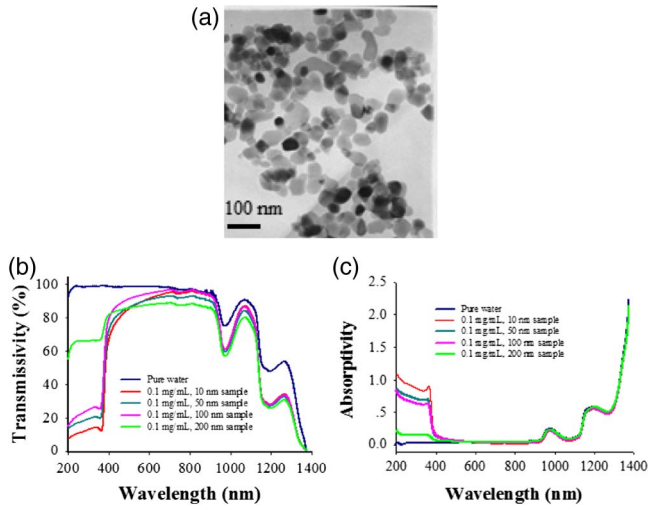


Fig. 1. (a) TEM image of ZnO nanospheres. (b) Transmission spectra of 1 cm pure water sample and four ZnO nanosphere/water samples. (c) Absorption spectra of 1 cm pure water sample and four ZnO nanosphere/water samples.

particle sizes at the same sample concentration of 0.1 mg/mL, respectively. Each experimental sample was put into a quadrangle optical cuvette with a 1 cm path length for the corresponding transmission and absorption spectra measurements by employing a SHIMADZU Solid-spec-3700 UV-VIS-NIR scanning spectrophotometer.

By comparing the transmission and absorption spectra of the ZnO nanosphere-water sample with the curve of a pure water sample, it can be seen that there is a distinct sharp attenuation band edge located at ~ 370 nm. The 1 cm length pure water sample presents two near-infrared absorption bands located at 974 and 1195 nm, and also, another strong absorption band is located at the wavelength of ~ 1400 nm. The characteristic absorption band of ZnO nanospheres in the UV region is ascribed to the intrinsic transition between the valence band (VB) and the conduction band (CB), which confirms that the as-prepared ZnO nanospheres present a crystalline nature. In this Letter, in order to reduce the absorption loss caused by the characteristic absorption band of ZnO nanospheres in the UV region, the incident wavelength was chosen to be 457 nm.

In this research, the scattering behaviors will be simply described by the aid of the Mie theory in a particle scattering system. The scattering behaviors from a nanosphere suspended in a homogeneous medium (particle scattering system) are well known and can be expressed as an infinite series^[2,26,27]:

$$\sigma_{\text{scat}} = \frac{\lambda^2}{2\pi} \sum_{n=1}^{\infty} (2n+1) (|a_n|^2 + |b_n|^2), \quad (1)$$

$$I_1 = \left| \sum_{n=1}^{\infty} \frac{2n+1}{n(n+1)} [a_n \pi_n(\cos \theta) + b_n \tau_n(\cos \theta)] \right|^2, \quad (2)$$

$$I_2 = \left| \sum_{n=1}^{\infty} \frac{2n+1}{n(n+1)} [a_n \tau_n(\cos \theta) + b_n \pi_n(\cos \theta)] \right|^2, \quad (3)$$

$$I = \frac{I_1 + I_2}{2}, \quad (4)$$

where n is a positive integer, I_1 and I_2 are the angular intensity functions of vertically and horizontally polarized light with respect to the scattering plane, respectively. $\lambda = \lambda_0/n_1$ is the wavelength of the incident light in the surrounding medium, λ_0 is the wavelength of the incident light, n_1 is the refractive index of the surrounding medium, π_n and τ_n are the angular dependent functions expressed in terms of the Legendre polynomials by

$$\pi_n(\cos \theta) = \frac{P_n^{(1)}(\cos \theta)}{\sin \theta}, \quad (5)$$

$$\tau_n(\cos \theta) = \frac{dP_n^{(1)}(\cos \theta)}{d\theta}. \quad (6)$$

The parameters a_n and b_n are two complex coefficients defined by

$$a_n = \frac{\Psi_n(\alpha) \Psi_n'(m\alpha) - m \Psi_n(m\alpha) \Psi_n'(\alpha)}{\zeta_n(\alpha) \Psi_n'(m\alpha) - m \Psi_n(m\alpha) \zeta_n'(\alpha)}, \quad (7)$$

$$b_n = \frac{m \Psi_n(\alpha) \Psi_n'(m\alpha) - \Psi_n(m\alpha) \Psi_n'(\alpha)}{m \zeta_n(\alpha) \Psi_n'(m\alpha) - \Psi_n(m\alpha) \zeta_n'(\alpha)}, \quad (8)$$

where $m = n_2/n_1$, n_2 is the refractive index of the spherical particle, and the size parameter α is defined by

$$\alpha = \frac{2\pi r}{\lambda}. \quad (9)$$

Here, r is the radius of spherical particle. Ψ and ζ are the Ricatti-Bessel functions and are defined by

$$\Psi_n(z) = \left(\frac{\pi z}{2}\right)^{1/2} J_{n+1/2}(z), \quad \Psi_n'(z) = \frac{\partial \Psi_n(z)}{\partial z}, \quad (10)$$

$$\zeta_n(z) = \Psi_n(z) + iX_n(z), \quad \zeta_n'(z) = \frac{\partial \zeta_n(z)}{\partial z}, \quad (11)$$

$$X_n(z) = -\left(\frac{\pi z}{2}\right)^{1/2} J_{-n-1/2}(z), \quad (12)$$

where $J_{n+1/2}(z)$ and $J_{-n-1/2}(z)$ are the half-integer-order Bessel functions, and z takes on the values of α or $m\alpha$.

When a monochromatic laser with the wavelength λ_0 is passing through the suspension of a spherical particle, the attenuation of the light intensity can be expressed as

$$I(\lambda_0, l) = I_0(\lambda_0) e^{-\alpha_1(\lambda_0)l} e^{-\alpha_2(\lambda_0)l}, \quad (13)$$

where $I_0(\lambda_0)$ is the initial intensity of the incident light, l is the propagation distance of light in the medium, $\alpha_1(\lambda_0)$ is the extinction coefficient of the surrounding medium at

the wavelength of λ_0 , and $\alpha_2(\lambda_0)$ is the extinction coefficient relating to the spherical particles at the wavelength of λ_0 . Based on Eq. (13), the transmittance of the incident light in the scattering system can be described by

$$T(\lambda_0) = \frac{I(\lambda_0, l)}{I_0(\lambda_0)} = e^{-\alpha_1(\lambda_0)l} e^{-\alpha_2(\lambda_0)l} = T_1(\lambda_0) e^{-\alpha_2(\lambda_0)l}. \quad (14)$$

Here, we define the parameter $T_1(\lambda_0)$ as the transmittance of the surrounding medium without the spherical particles. Generally, α_2 is related to the absorption and scattering of the nanoparticles. In this Letter, we have measured the absorption coefficients of pure water and ZnO scattering samples [shown in Fig. 1(b)]. The measured results show that the absorption coefficient of the ZnO particles is much lower than the absorption coefficient of pure water and can be neglected. Then, the scattering extinction coefficient of the suspension medium can be expressed by

$$\alpha_{\text{scat}}(\lambda_0) = \alpha_2(\lambda_0) = \frac{1}{l} \ln \left[\frac{T_1(\lambda_0)}{T(\lambda_0)} \right]. \quad (15)$$

When the wavelength of the incident light is smaller than the average distance between the spherical particles, the relation between the scattering extinction coefficient $\alpha_{\text{scat}}(\lambda_0)$ and the scattering cross section $\sigma_{\text{scat}}(\lambda_0)$ can also be expressed simply as

$$\alpha_{\text{scat}}(\lambda_0) = N\sigma_{\text{scat}}(\lambda_0), \quad (16)$$

where N is the spherical particle number per cubic centimeter.

It is generally known that the scattering of light by very small, sub-wavelength-sized particles (where the particle size is much smaller than the wavelength of the incident light) is often called Rayleigh scattering. If the particle size is comparable to the incident wavelength (normally, it is approximately greater than 1/20 the incident wavelength), the scattering of light from the particles can be classified as Mie scattering. In order to make a comparison between Rayleigh scattering and Mie scattering, two samples of pure water and ZnO nanosphere/water (particle scattering system) were prepared. Figure 2 shows the side view of a laser-induced light scattering phenomenon from the pure water sample and a 50 nm ZnO nanosphere/water sample with 0.1 mg/mL concentration.

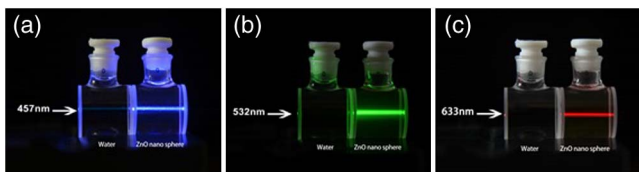


Fig. 2. Mie scattering in ZnO sample and Rayleigh scattering in pure water at three different incident wavelengths. (a) Incident wavelength 457 nm. (b) Incident wavelength 532 nm. (c) Incident wavelength 633 nm.

The incident laser beams holds the same energy but with three different wavelengths of 457, 532, and 633 nm. These photos were taken with the same exposure time. From Fig. 2 we can see that the Rayleigh scattering from the pure water sample was more obvious at short wavelengths than at long wavelengths. Meanwhile, the intensity of the Mie scattering from the ZnO nanosphere/water sample is much stronger than the Rayleigh scattering from a pure water sample. Based on the scattering phenomenon from the ZnO nanosphere/water sample, the angular distribution of the scattering intensity has been analyzed and is presented in the following sections.

In order to measure the angular distribution of the scattering intensity from ZnO nanosphere/water samples with different particle sizes, the optical setup shown in Fig. 3 was employed. The wavelength of the incident laser was 457 nm with a 45° linear polarization relative to the observation plane. The tested sample was put into a cylindrical cuvette with a 10 mm inner diameter, and a photodiode detector was set around the cuvette at the same distance over a range of 0°–360°.

The measured results of the normalized angular distribution of the scattering intensity from four ZnO nanosphere/water samples with different particle diameters is shown in Fig. 4, which was obtained at the same sample concentration of 0.1 mg/mL. The scattering light was measured every 10°, and each point is an average result of 20 measured values. It is necessary to state that because of the limit of the propagation direction of the incident light, the measured scattering intensity at the zero scattering angle was replaced by the measured scattering intensity in the ~3°–5° direction. In order to make a comparison with the experimental measurements, the angular distribution of the scattering intensity was simulated using the Mie theory. For a natural polarized light or two equal polarized beams along the vertical and parallel directions, the angular distribution of the average scattering intensity can be calculated by Eq. (4). Figure 5 shows the normalized angular distribution curves of the scattering intensity in a polar plot, using the conditions of a 457 nm wavelength and four different particle diameters of $R = 10, 50, 100,$ and 200 nm. We can see from Fig. 5

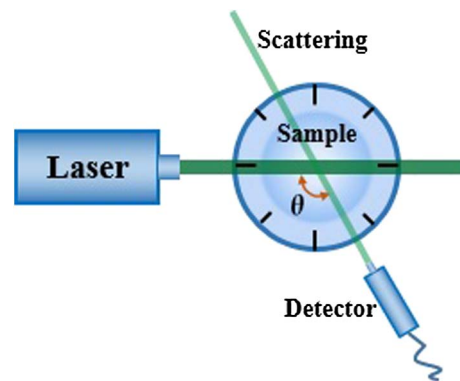


Fig. 3. Experimental setup for measuring the angular distribution of the scattering intensity.

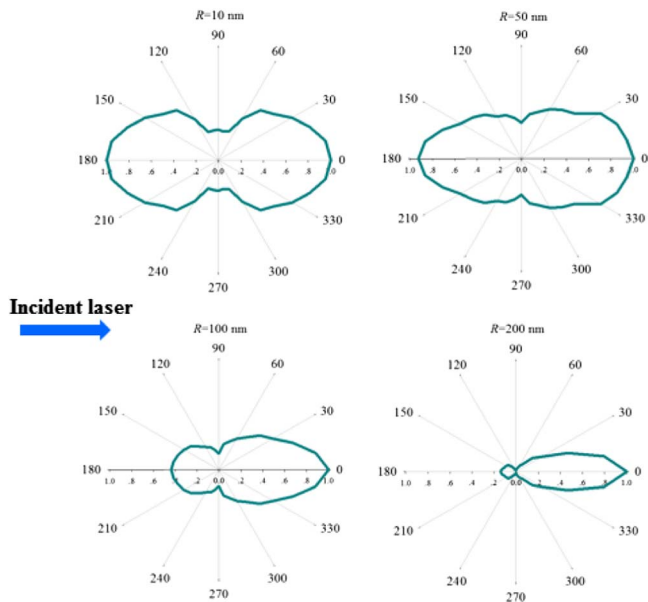


Fig. 4. Measured normalized angular distribution curves for four scattering samples with different particle diameters. The blue arrow denotes the propagation direction of the incident laser.

that the angular distribution of the scattering intensity becomes gradually asymmetric between the forward and the backward directions. The scattering intensity of the forward direction increases with the increase of the particle diameter R , but the backward-scattering intensity diminishes gradually with the increase of the particle

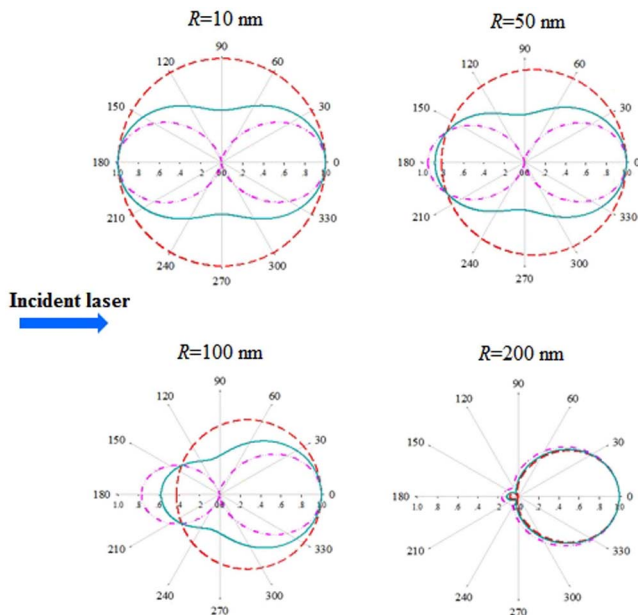


Fig. 5. Calculated normalized angular distribution of scattering intensity of four scattering samples with different particle diameters. The long dashed lines, dashed-dotted lines, and solid lines represent that the polarization of the incident light is vertical linear polarization (I_1), parallel linear polarization (I_2), and 45° linear polarization (or naturally polarized light, $I_1 + I_2/2$), respectively.

diameter. By comparing the theoretical and experimental results, it can be seen that the measured angular distribution of the scattering intensity from the ZnO nanosphere/water sample presents nearly the same variation trend with the curve simulated by Eq. (4). Compared with the theoretical simulation, in the measured scattering intensity there exists a small difference. The reason for this deviation is mainly caused by the intensity attenuation due to the sample cell and the additional optical components.

In order to more visually show the relationship between the scattering intensity and the scattering angle and the particle size, Fig. 6 gives a three-dimensional (3D) plot of the calculated angular distribution of the scattering intensity. It can be seen that the relationship presents a symmetrical 3D curved surface. The backward-scattering intensity decreases with the increase of the particle size, the forward-scattering intensity will gradually become dominant, and it is more obvious when the particle size is larger. This is similar to the result shown in Fig. 5. In fact, when the particle size $R \leq 10$ nm, the angular distribution of the scattering intensity is nearly symmetrical and can also be described by the Rayleigh scattering theory in a pure molecular medium: $I = (1 + \cos^2 \theta)/2$ (here, θ denotes the scattering angle).

As can be seen from the measured and simulated angular distributions of the scattering intensity, the scattering behavior presents a forward radiative transfer phenomenon with the increase of the particle diameter. This phenomenon can also be observed from the viewing plane shown in Fig. 7, in which the scattering light appears as a clearly forward-propagating feature when the particle diameter increases from 10 to 200 nm at the same incident laser wavelength, and the forward-scattering intensity is dominant gradually. To provide a basis for better understanding certain scattering behaviors, the comparisons between the experimental results and the theoretical predictions of the scattering extinction coefficient and the scattering cross section of ZnO samples have been provided in the following paragraphs.

For a certain incident wavelength, the scattering extinction coefficient can be determined based on Eq. (15) through measuring the transmittance changes of a 1 cm

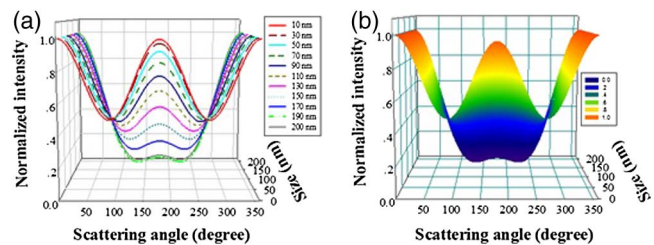


Fig. 6. 3D plot of the normalized angular distribution of scattering intensity versus the scattering angle and the particle size. (a) 3D line plot. (b) 3D mesh plot. The direction of the 0° or 360° scattering angle represents the propagation direction of the incident laser.

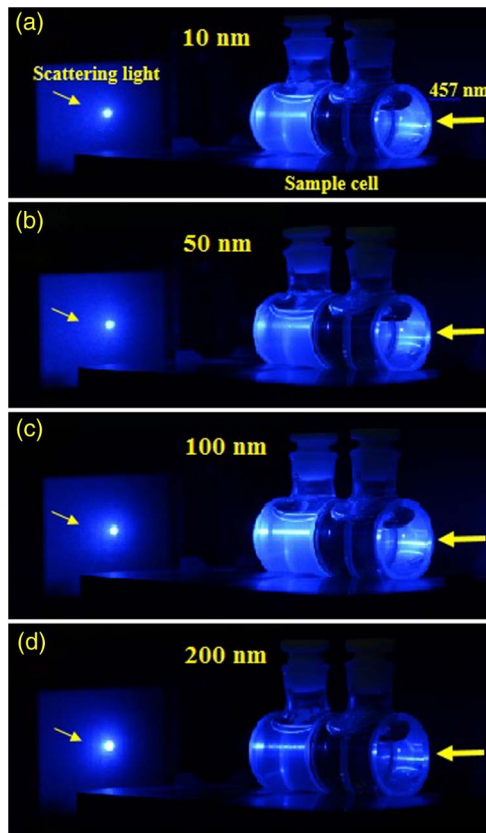


Fig. 7. Photos for observing the change of forward scattering of four samples with different particle diameters. The wavelength of the incident laser is 457 nm. The horizontal yellow arrows represent the direction of the incident laser.

pure water sample and a 1 cm ZnO sample with a given particle diameter. The measured curves of the scattering extinction coefficients of four different samples versus the wavelengths are shown in Fig. 8(a). From Fig. 8(a), we can see that the scattering extinction coefficient decreases with the increase of the wavelength for the same particle size over the entire visible range; for a certain wavelength, the larger the particle size is, the larger the extinction coefficient is. We can also draw the same conclusion from Fig. 8(b) for three given wavelengths at 457, 532, and 633 nm. It needs to be noted that at the near-infrared region, two apparent extinction bands located at 974 and 1195 nm were attributed to the strong absorption of water.

Based on Eq. (16), the scattering cross section as a function of the wavelength can be obtained by using the

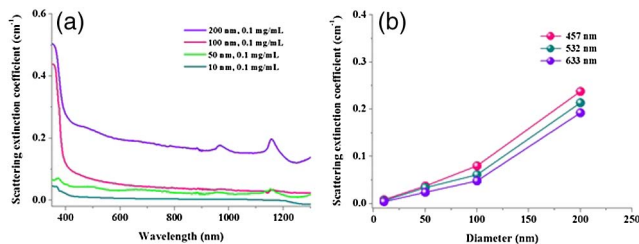


Fig. 8. Scattering extinction coefficients of four different ZnO samples.

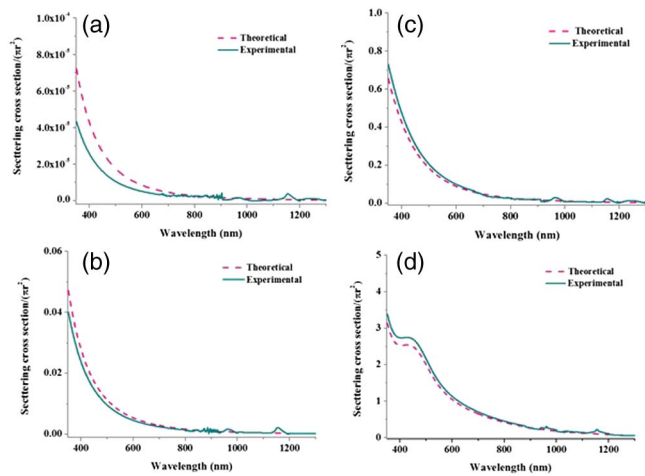


Fig. 9. Experimental and theoretical curves of scattering cross sections of four different ZnO samples versus the wavelength. The corresponding particle diameters are (a) 10, (b) 50, (c) 100, and (d) 200 nm.

extinction coefficient shown in Fig. 8 and the number density N of the nanospheres for a given sample concentration. Figure 9 shows the experimental results and theoretical predictions of the scattering cross section from four ZnO samples with different particle diameters. One can see that the scattering cross section decreases with the increase of wavelength for all four scattering samples within the given wavelength region (visible and near-infrared range). From Fig. 9 it can be seen that the experimental results agree well with the theoretical predictions in addition to the result of the ZnO sample with the 10 nm particle diameter. For the scattering properties of spherical particles with 10 nm diameters, the Rayleigh scattering theory is more suitable to characterize them well than the Mie scattering theory.

For comparison, shown in Fig. 10 is the scattering cross section of four scattering samples at three given wavelengths of 457, 532, and 633 nm. From Fig. 10, one can notice the following two features: (i) the scattering cross section increases with the increase of the particle diameter

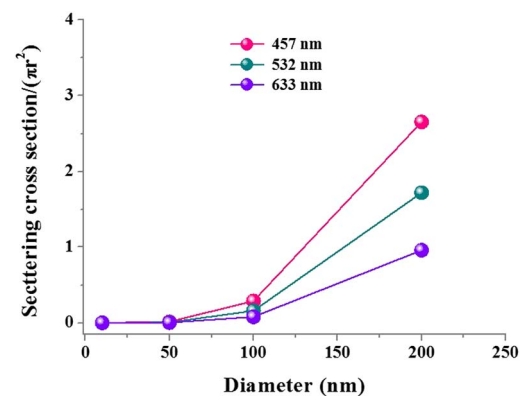


Fig. 10. Scattering extinction sections of four ZnO samples at the three given wavelengths.

at the same incident wavelength, and (ii) at the same particle diameter, the shorter wavelength corresponds to a larger scattering cross section, which was particularly evident when the diameter of the ZnO nanosphere was 200 nm.

It must be emphasized that the light scattering is sensitive to all microstructural properties (size, shape, orientation distribution, interparticle interaction, etc.) of scattering particles. The contents presented in this Letter are just a special description for the scattering properties of four different sizes of ZnO nanoparticles. In a real case, the scattering properties of large-sized microstructural particles become difficult to interpret by an approximate Mie scattering theory. For example, a Tyndall scattering criterion might be more suitable to describe the scattering behaviors when the particle size reaches the magnitude of microns. As for other microstructural parameters, i.e., orientation distribution and interparticle interaction, their influences on the scattering behaviors of nanoparticles are beyond the scope of this work.

In conclusion, we experimentally and theoretically investigate the light scattering properties of ZnO nanospheres suspended in water in a given spectral range from 400 to 1300 nm. The particle sizes of the ZnO nanospheres used in this experiment are 10, 50, 100, and 200 nm. The angular distributions of the scattering intensity, scattering extinction coefficient, and scattering cross section are simulated in a way that can explain the experimental results well. The transmission spectrum of a given scattering sample can be used to determine the scattering extinction coefficient and the scattering cross section. The theoretical simulation and experimental measurement results demonstrate the size, angle, and wavelength dependences of ZnO nanospheres suspended in water. This proposed method may be helpful to study the refractive index change behavior of nanoparticles suspended in a liquid medium.

This work was supported by the National Natural Science Foundation of China (Nos. 41666004, 41576033, and 61465009) and the Graduate Student Innovation Foundation of Jiangxi Province (No. YC2015-S331).

References

1. L. Rayleigh, *Philos. Mag.* **47**, 375 (1899).
2. G. Mie, *Ann. Phys.* **330**, 377 (1908).
3. J. Tyndall, *Proc. R. Soc. London* **17**, 223 (1868).
4. E. I. Franses, J. M. Caruthers, and S. Yarlagadda, *J. Chem. Phys.* **83**, 1531 (1985).
5. T. Wriedt, *Part. Part. Syst. Char.* **15**, 67 (1998).
6. T. Wriedt, *J. Quantum Spectrosc. RA.* **110**, 833 (2009).
7. G. Gouesbet, F. Xu, and Y. P. Han, *J. Quantum Spectrosc. RA.* **112**, 2249 (2011).
8. B. Schmidtke and E. A. Rössler, *J. Chem. Phys.* **141**, 044511 (2014).
9. B. Kang, Y. Cai, and L. Wang, *Chin. Opt. Lett.* **14**, 070401 (2016).
10. M. Hlaing, B. Gebear-Eigzabher, A. Roa, A. Marciano, D. Radu, and C. Y. Lai, *Opt. Mater.* **58**, 439 (2016).
11. I. Kim, K. S. Lee, T. S. Lee, D. S. Jung, W. S. Lee, W. M. Kim, and K. S. Lee, *Synthetic Met.* **199**, 174 (2015).
12. S. Eustis and M. A. El-Sayed, *Phys. Chem. B* **109**, 16350 (2005).
13. K. Aslan, P. Holley, L. Davies, J. R. Lakowicz, and C. D. Geddes, *J. Am. Chem. Soc.* **127**, 12115 (2005).
14. G. S. He, H. Y. Qin, and Q. Zheng, *J. Appl. Phys.* **105**, 023110 (2009).
15. G. S. He, K. T. Yong, J. Zhu, and P. N. Prasad, *Phys. Rev. A* **85**, 043839 (2012).
16. P. J. Wyatt, *Anal. Chem.* **86**, 7171 (2014).
17. M. I. Mishchenko, L. D. Travis, and A. A. Lacis, *Scattering, Absorption, and Emission of Light by Small Particles* (NASA Goddard Institute for Space Studies, 2002).
18. J. Shi, H. Wu, F. Yan, J. Yang, and X. He, *J. Nanopart. Res.* **18**, 23 (2016).
19. P. K. Jain, K. S. Lee, I. H. El-Sayed, and M. A. El-Sayed, *J. Phys. Chem. B* **110**, 7238 (2006).
20. C. Ding, K. Yang, W. Li, W. Guo, X. Zhang, and M. Xia, *Opt. Laser Technol.* **62**, 135 (2014).
21. T. Honda, M. Terakawa, and M. Obara, *Appl. Phys. B* **111**, 117 (2013).
22. A. A. Tomchenko, G. P. Harmer, B. T. Marquis, and J. W. Allen, *Sens. Actuators B* **93**, 126 (2003).
23. S. H. Chen, U. Nickel, and X. M. Ren, *J. Colloid Interface Sci.* **176**, 286 (1995).
24. S. Chen, J. Shi, X. Kong, Z. Wang, and D. Liu, *Laser Phys. Lett.* **10**, 055006 (2013).
25. S. J. Chen, Y. Zhou, T. R. Zhai, Z. N. Wang, and D. H. Liu, *Laser Phys. Lett.* **9**, 570 (2012).
26. W. Liben and B. Goldberg, *J. Opt. Soc. Am.* **43**, 347 (1953).
27. M. Born and E. Wolf, *The Principles of Optics* (Pergamon, 1980).